# Molecular and Functional Analysis of Calcium Binding by a Cancer-linked Calreticulin Mutant

**Ishmael Nii Ayibontey Tagoe**[1, 2], **Amanpreet Kaur** [1], **Osbourne Quaye**[2], **Emmanuel Ayitey Tagoe**[4], **Nicole Koropatkin**[1], **Leslie S. Satin**[3], **and Malini Raghavan**[1]*

[1]Departments of Microbiology and Immunology and [3]Pharmacology,

University of Michigan Medical School, Ann Arbor, MI

[2]West African Centre for Cell Biology of Infectious Pathogens,

Departments of Biochemistry, Cell and Molecular Biology, and

[4]Medical Laboratory Sciences, University of Ghana

*Correspondence to Malini Raghavan, PhD: malinir@umich.edu

**Abstract**

Calreticulin (CRT) is an endoplasmic reticulum (ER) chaperone with low affinity calcium binding sites in its C-terminal domain. This region is altered by somatic mutations in the CRT gene (*CALR*), which drive a subset of myeloproliferative neoplasms (MPN). Perturbations in ER calcium storage and signaling are reported for the MPN type I mutant, $CRT_{Del52}$, and are linked to disease pathogenesis. Using recombinant CRT proteins, we found similar low affinity calcium binding characteristics for wild-type CRT and $CRT_{Del52}$, as determined by isothermal titration calorimetry (ITC). Residues 340–349, conserved in both wild-type CRT and $CRT_{Del52}$, contribute to binding. Furthermore, ER and cytosolic calcium levels and store-operated calcium entry (SOCE) were comparable in CRT knockout (CRT-KO) cells reconstituted with wild-type CRT or $CRT_{Del52}$. Notably, the CRT-KO induces expression of multiple ER proteins known to contain low affinity calcium binding sites or regulate ER calcium levels. Overall, these findings indicate that $CRT_{Del52}$ retains at least some low affinity calcium binding capacity and that CRT-deficiency induces compensatory cellular changes that maintain ER calcium homeostasis.

**Summary**

Pathogenic $CRT_{Del52}$ retains at least partial low-affinity calcium-binding capacity. Additionally, live-cell imaging and flow cytometry with ratiometric calcium probes indicate that ER and cytosolic calcium levels, as well as store-operated calcium entry (SOCE), are comparable in CRT-deficient cells rescued with either wild-type CRT or $CRT_{Del52}$.

## Introduction

Calreticulin (CRT) is an endoplasmic reticulum (ER) luminal protein that plays key roles in the assembly and folding of N-linked glycoproteins. CRT has a highly acidic C-terminal domain that contains multiple low affinity calcium binding sites (Baksh and Michalak, 1991, Wijeyesakere et al., 2011). As an ER chaperone, CRT is thought to play a critical role in maintaining cellular calcium homeostasis (Venkatesan et al., 2021b, Michalak, 2024). The ER has a relatively high free calcium concentration of 0.5-1 μM through the presence of various low affinity calcium-binding proteins that buffer calcium, whereas cytosolic calcium levels are maintained within a narrow range of around 100 nM (Michalak, 2024). The maintenance of calcium homeostasis within cellular compartments is essential for cell function and survival (Bagur and Hajnoczky, 2017). Early studies have shown that the C-domain of CRT contributes to ER calcium storage, although free ER luminal concentrations are unchanged (Nakamura et al., 2001).

Somatic mutations of exon 9 of the *CALR* gene including a 52-base pair deletion (Del52; type 1 mutation) and a 5-base pair insertion (Ins5; type 2 mutation), are driver mutations in some myeloproliferative neoplasms (MPN), specifically in essential thrombocythemia (ET) and primary and secondary myelofibrosis (PMF) (Klampfl et al., 2013, Nangalia et al., 2013). The MPN mutations change the CRT C-domain residues from being predominantly acidic to a high prevalence of basic amino acids and result in a loss of the ER-retention KDEL sequence (Klampfl et al., 2013, Nangalia et al., 2013). Although all MPN CRT mutants change the sequence and charge of the C-domain, a greater number of acidic residues are retained in MPN type 2 mutant ($CRT_{Ins5}$), compared to the type I mutant ($CRT_{Del52}$)**.** The loss of more acidic residues from the C-terminal domain of $CRT_{Del52}$ has been reported to impair its calcium binding and reduce ER calcium levels (Ibarra et al., 2022). Store-operated calcium entry (SOCE) is a physiological process that allows for the entry of extracellular calcium and ER calcium restoration following ER calcium depletion (Putney, 2011, Zhang et al., 2020). Altered calcium release from the ER and SOCE was reported for MPN type I but not type 2 mutants in cultured megakaryocytes from MPN patients (Pietra et al., 2016). In another study, spontaneous calcium spikes and increased SOCE activation were observed in cultured megakaryocytes from MPN type I and type 2 patients when compared to healthy donors (Di Buduo et al., 2020).

Although global calcium binding defects were predicted or qualitatively measured for $CRT_{Del52}$ (Shivarov et al., 2014, Ibarra et al., 2022) and altered cellular calcium signaling is also reported (Pietra et al., 2016, Di Buduo et al., 2020), it remains unclear whether MPN-linked $CRT_{Del52}$ has any low affinity calcium binding capacity, given that a few conserved acidic residues are retained in its C-domain (Figure 1). In fact, our previous studies showed that a truncated version of murine wild-type CRT (mCRT) containing the non-mutated part of $CRT_{Del52}$ and two additional C-terminal residues ($mCRT_{1-351}$) showed similar low affinity calcium binding characteristics as the wild-type mCRT (Wijeyesakere et al., 2011). On the other hand, further truncation of mCRT ($mCRT_{1-339}$) was needed to disrupt calcium binding (Wijeyesakere et al., 2011, Wijeyesakere et al., 2016). The goal of the current study was to quantitatively measure low affinity calcium binding by $CRT_{Del52}$ compared with wild-type human CRT and also quantify ER and cytosolic calcium levels and calcium responsiveness in cells expressing wild-type CRT or $CRT_{Del52}$.

## Material and Methods

### Protein expression and purification

B1 domain of streptococcal protein G (GB1) and his-tagged versions of wild-type CRT, $CRT_{(1-351)}$, $CRT_{(1-339)}$ and $CRT_{Del52}$ were purified following expression in *E. coli* cells using a nickel resin and gel filtration chromatography as described previously (DelProposto et al., 2009, Del Cid et al., 2010, Wijeyesakere et al., 2011) (also see supplemental methods). The monomer fractions were pooled, dialyzed and concentrated to 4 mg/mL in buffer containing 20 mM HEPES, 10 mM NaCl 1 mM $CaCl_2$ pH 7.5 using Amicon ultra concentrators with a molecular weight cut-off of 30,000 Dalton (Millipore) and frozen in 10% glycerol for further use.

### Isothermal titration calorimetry

Isothermal titration calorimetry (ITC) measurements were done using the Nano-ITC SV (TA Instruments). Purified CRT monomers were dialyzed into 20 mM HEPES, 10 mM NaCl pH 7.5, brought to a concentration of 100 μM, and then pre-incubated with 50-100 μM $CaCl_2$ in 20 mM HEPES, 10 mM NaCl pH 7.5 for 30 minutes to block the high affinity calcium binding sites. This was followed by 25 sequential 10μL injections of 20 mM HEPES, 10 mM NaCl, 10 mM $CaCl_2$ pH 7.5 into the protein solutions maintained at 37°C. The heat changes measured for the sequential injections were curve-fitted to calculate the enthalpies, stoichiometries, and the dissociation constants using NanoAnalyze software.

### Cytosolic calcium measurement and store-operated calcium entry (SOCE) induction

MEG-01 cells and their *CALR*-modified versions (see supplemental methods) were plated on glass coverslips pretreated with 0.01% poly-L-lysine to facilitate cell attachment. Cells were loaded with 2.5 μM Fura-2/AM dye (Ion Biosciences) supplemented with 0.1% pluronic acid in a physiological salt solution (PSS) containing 140 mM NaCl, 2 mM $CaCl_2$, 5 mM KCl, 2 mM $MgCl_2$, 10 mM HEPES and 11 mM glucose, and incubated for 60 minutes at 37°C. Live single-cell imaging was done at 20X magnification using an Olympus IX71 inverted microscope equipped with a TILL Polychrome V monochromator light source, a Dual-View emission beam splitter, and a cooled Photometrics Quant-EM camera. Cells were transferred to a perfusion chamber that was mounted on the microscope stage, and PSS with or without 2 mM $CaCl_2$ was flowed over cells using a gravity-fed perfusion system. Cytosolic calcium measurements were performed by perfusing Fura-2 loaded cells in the chamber with 2 mM $Ca^{2+}$, followed by the addition of 25 μM cyclopiazonic acid (CPA) (Cayman) into the imaging buffer. To determine cytosolic calcium levels after activating SOCE, cells were initially perfused with $Ca^{2+}$-free PSS containing 0.1 mM EGTA, followed by the addition of 25 μM CPA in $Ca^{2+}$-free PSS and subsequent addition of 2 mM $Ca^{2+}$ and 25 μM CPA in PSS (without EGTA) to reestablish calcium influx. The emission signals corresponding to the 340 and 380 nm excitation were recorded, and the signals resulting from 340/380 nm excitation were calculated using the Meta Fluor software. The basal cytosolic calcium was defined as the 340/380 nm signal ratio before CPA treatment (measured over a 4- or 5-minute interval immediately before CPA addition). The fractional increase in cytosolic calcium levels after ER $Ca^{2+}$ depletion with CPA was calculated as the difference between peak signal (single time point) and baseline (averaged over a 4- or 5-minute interval before CPA addition), as a ratio relative to the baseline. The fractional increase in cytosolic calcium after addition of 2 mM extracellular $Ca^{2+}$ and CPA was calculated as the difference between the peak signal following $Ca^{2+}$ and CPA addition (averaged over a 1-minute time interval following the peak signal) and the baseline (the signal averaged over a 0.8-1-minute interval immediately before the $Ca^{2+}$ and CPA addition) relative to the baseline. Total calcium release after ER $Ca^{2+}$ depletion was reported as the total area under the curve (AUC). Fractional increases were calculated as (Peak-Baseline)/Baseline x 100. This was calculated as

peak signals after CPA addition relative to the baseline before CPA (measured over a 4- or 5-minute interval immediately before CPA addition).

**ER calcium measurements in HEK293T cells**

*CALR*-modified HEK cells were prepared as described in supplemental methods. Cells were transiently transfected with pCIS-GEM-CEPIA1er (Suzuki et al., 2014); Addgene plasmid # 58217) using Fugene HD reagent (Promega). The transfected cells were harvested after 72 hours. Cells were washed twice with FACS buffer (PBS + 2% FBS) supplemented with 2 mM $Ca^{2+}$ and resuspended in the same FACS buffer. The live-dead stain 7-AAD (BD) was added at 1:200 dilution and the cells were analyzed by flow cytometry using the BD LSRFortessa cell analyzer. The signal for the $Ca^{2+}$-bound GEM-CEPIA1er probe was recorded in the Pacific Blue channel (excitation at 405 nm and emission at 452-455 nm) and the signal for the unbound probe was recorded in the AmCyan channel (excitation at 405 and emission at 498 nm). The analysis of flow cytometry data was done in the FlowJo software (v10.10.00). The cells were gated based on the forward (FSC-A) and side scatter (SSC-A), followed by gating on the 7AAD-negative (live) cells, and subsequent gating on the cells positive for the expression of GEM-CEPIA1er probe measured in the Pacific Blue and AmCyan channels. Basal signals were initially recorded, followed by the addition of 5 μM thapsigargin (Tg) and subsequent recording of signals for the treated and untreated cells at four different time points between 2 – 10 minutes. The ratio of mean fluorescence intensity (MFI) of the bound to the unbound signal was used for calculations.

**RNA-sequencing**

The parental and CRT-KO MEG-01 cells were grown in complete media for 12-18 hours before harvesting. Total RNA was isolated using the RNeasy Plus Mini Kit (Qiagen). This was followed by poly-A selection and enrichment of mRNA using NEB Next Ultra Express RNA kit and a NEB Poly A kit (New England Biolabs). Sequencing was done on the NovaSeq at PE150, targeting 30-40 million reads/sample after cDNA library preparation. Data were pre-filtered to remove genes with 0 counts in all samples. Differential gene expression analysis was performed using DESeq2. The differentially expressed genes were selected as those with a log2 fold-change of <-0.49 or >0.49 and p values <0.05. The results from RNA sequencing were further analyzed in the iPathwayGuide to identify significantly altered proteins related to calcium signaling. The volcano plot was plotted in GraphPad Prism as Log2 fold-change (x-axis) *vs.* -Log10 adjusted p-value.

**Real-time polymerase chain reaction**

Total RNA was isolated using the RNeasy Plus Mini Kit (Qiagen) followed by synthesis of complementary DNA using the Superscript III First-Strand Synthesis Kit (ThermoFisher Scientific) following the manufacturer's protocol. Quantitative RT-PCR was performed on the ABI 7500 FAST Real Time PCR machine (ThermoFisher Scientific, USA) using the SYBR Green PCR Master mix (Applied Biosystems, UK) and gene-specific primers (Supplementary Table 2). Measurement was done in technical duplicates. The expression of target genes was quantified using the $2^{-\Delta\Delta Ct}$ method and normalized to the expression of either one or multiple endogenous control genes including beta-actin (ACTB), glyceraldehyde 3-phosphate dehydrogenase (GAPDH) and hypoxanthine phosphoribosyltransferase 1 (HPRT1). The expression of the target gene in MEG-01 CRT-KO and wild type and $CRT_{Del52}$ reconstitution cells was further normalized to the mean expression of parental MEG-01 or CRT-KO-vec. The calculated relative mRNA transcript expression values (RQ) were plotted using GraphPad Prism.

## Results

### MPN-linked $CRT_{Del52}$ retained at least some low affinity calcium binding sites

Previous studies (Wijeyesakere et al., 2011) have implicated residues 340 to 351 of murine CRT, which are identical in wild-type human CRT and fully conserved with the 340 to 349 residues of $CRT_{Del52}$, to be involved in low affinity calcium binding. Further truncation of the C-domain to the residue 339 ($mCRT_{1-339}$) led to the loss of calcium binding measured by ITC (Wijeyesakere et al., 2011). Figure 1 shows a sequence alignment of murine CRT, human CRT, $CRT_{Ins5,}$ and $CRT_{Del52}$ proteins and indicates that the residues previously implicated in low affinity calcium binding are also shared between wild-type CRT and $CRT_{Del52}$. Recombinant his and GB1 tagged purified proteins were used to compare calcium binding by human CRT and its variants. Chromatograms for human wild-type CRT, $CRT_{Del52}$, $CRT_{(1-339)}$ and $CRT_{(1-351)}$ are shown in Figure 2A. SDS-PAGE gels corresponding to the purified proteins are shown in Figure 2B. $CRT_{Ins5}$ was not purified in sufficient quantities needed for ITC experiments and was not further investigated in this study.

For the ITC measurements, calcium titrations were performed after pre-blocking the high affinity calcium binding sites with 50-100 μM $CaCl_2$. Similar binding profiles and properties were observed with wild-type CRT, $CRT_{Del52,}$ and the $CRT_{(1-351)}$ mutant (Figures 3A, C and D and Table 1). However, consistent with previous studies with $mCRT_{(1–339)}$, endothermic calcium binding by human $CRT_{(1–339)}$ was of lower magnitude compared to other constructs, with a $K_D$ value that was too low to be reliably fit, suggesting the loss of low affinity calcium binding sites in this mutant (Figure 3B and Table 1). There are exothermic peaks observed with human $CRT_{(1–339)}$ at the beginning of the calcium titration, which may be attributed to altered low affinity sites retained within the mutant or reduced affinity of the high affinity sites. We concluded that $CRT_{Del52}$ retains low affinity calcium binding that is measurable by ITC.

### Similar ER calcium levels in CRT-KO HEK cells reconstituted with wild-type CRT or $CRT_{Del52}$

While the $CRT_{Del52}$ mutant retains some ability to bind calcium (Figure 3 and Table 1), the loss of the ER-retention KDEL sequence induced by the frameshift mutation, which results in the secretion of the protein from the ER (Araki et al., 2016, Chachoua et al., 2016, Han et al., 2016, Arshad and Cresswell, 2018, Liu et al., 2020, Masubuchi et al., 2020, Venkatesan et al., 2021a, Pecquet et al., 2023) might be expected to cause ER calcium insufficiency in cells expressing $CRT_{Del52}$ compared to wild-type CRT. We investigated ER calcium signals in CRT knock-out HEK293T cells generated by CRISPR/Cas9 gene editing. A clonal KO line was generated and subsequently reconstituted with constructs encoding wild-type CRT, $CRT_{Del52}$, or $CRT_{Del52}$ with a KDEL sequence added at the C-terminus ($CRT_{Del52-KDEL}$). Protein expression was assessed by immunoblotting with anti-CRT(N), which detects an N-domain epitope present in all CRT constructs, and anti-CRT(C-mut), which was specifically raised against the mutant CRT C-terminus (Venkatesan et al., 2021a). While the recognition with anti-CRT (N) was very weak in lysates of cells expressing $CRT_{Del52,}$ which is secreted, $CRT_{Del52-KDEL}$ is readily detectable with both antibodies. Both wild-type CRT and $CRT_{Del52-KDEL}$ were reconstituted to higher levels than in the parental cells (Figure 4A**,** lanes 1 and 2 compared to 7-8 and 11-12). The KO and reconstituted cells were further transfected with pCIS-GEM-CEPIA1er, which encodes a ratiometric ER calcium probe (Suzuki et al., 2014). Emission signals for calcium-bound (452-455 nm) and unbound (498 nm) probe were measured using flow cytometry in the Pacific Blue and

AmCyan channels, respectively, following excitation with the 405 nm (violet) laser. Flow cytometric analysis was undertaken in a buffer containing 2 mM extracellular $Ca^{2+}$ (Figures 4B and 4C). There was a significant decrease in basal free ER calcium, measured by the bound/unbound ratios in CRT-KO cells compared to the parental cells, (Figure 4D, left panel). ER calcium levels were partially restored, although non-significantly, when the CRT-KO cells were reconstituted with wild-type CRT. CRT-KO cells reconstituted with $CRT_{Del52}$ and $CRT_{Del52\text{-}KDEL}$ showed small but non-significant decreases in ER calcium levels compared to those reconstituted with wild-type CRT (Figure 4D, right panel). Changes to ER calcium levels in response to thapsigargin (Tg), a SERCA inhibitor, were similar in the parental *vs.* CRT-KO cells, and in the CRT-KO cells compared with those reconstituted with different CRT proteins (Figure 4E).

**Similar cytosolic calcium and SOCE signals in a CRT-KO megakaryocyte cell line reconstituted with wild-type CRT or $CRT_{Del52}$**

MPN CRT mutations cause thrombopoietin-independent differentiation of megakaryocytes to platelets via the thrombopoietin receptor (MPL) (Araki et al., 2016, Chachoua et al., 2016, Marty et al., 2016, Li et al., 2018, Masubuchi et al., 2020). We, therefore, used a megakaryoblast cell line, MEG-01, to assess the role of CRT deficiency and the $CRT_{Del52}$ mutant on basal cytosolic calcium levels and SERCA inhibition-induced calcium influx into the cytosol. As with the HEK cells (Figure 4), we created a stable CRT knockout clone of MEG-01 cells by CRISPR/Cas9 editing for cytosolic calcium measurements. The cells were subsequently reconstituted with wild-type CRT or $CRT_{Del52}$. Representative immunoblots are shown to demonstrate the successful knockout and reconstitution (Figure 5A). Wild-type CRT reconstitution in MEG-01 CRT-KO cells resulted in expression levels higher than those in the parental cells (Figure 5A, lanes 7 and 8 compared with lanes 1 and 2). In the presence of 2 mM $Ca^{2+}$ in the media, we observed no significant differences in the basal cytosolic calcium levels or CPA-induced calcium release from ER in CRT-KO cells compared to the parental MEG-01 cells (Figure 5C and 5D). Additionally, no significant differences in basal cytosolic calcium were observed in CRT-KO cells compared to those reconstituted with wild-type CRT or $CRT_{Del52}$ (Figure 5E). Furthermore, cytosolic calcium levels in CRT-KO and the two reconstituted cell lines were not statistically different following CPA treatments.

SOCE is an important process for restoring ER calcium and maintaining intracellular calcium levels. In contrast to cytosolic calcium signals in the presence of 2 mM $Ca^{2+}$ in the media, in calcium-free saline, CRT-KO cells exhibited a small but significant increase in basal cytosolic calcium levels relative to the parental cells (Figure 6A, left panel and 6B). Upon ER calcium depletion with CPA, the mean fractional increase in the cytosolic calcium measured in the $Ca^{2+}$-free saline did not differ significantly in parental cells *vs*. CRT-KO cells. The areas under the curve were also not different for the two cell lines (Figures 6A and 6C). However, consistent with the higher basal cytosolic calcium measured in CRT-KO cells in calcium-free saline, the measured SOCE signal (following the addition of 2 mM $Ca^{2+}$ and CPA) was significantly reduced in CRT-KO cells compared to parental cells (Figure 6D). Reconstitution of the CRT-KO cells with either wild-type CRT or $CRT_{Del52}$ tended to reduce basal cytosolic calcium and induce SOCE (Figure 6A, right panel, 6E and 6G), but both trends were non-significant compared to CRT-KO cells. Importantly, there were no significant differences between the wild-type CRT and $CRT_{Del52}$ reconstituted cells, in either their basal or CPA-induced cytosolic calcium signals or in SOCE (Figures 6E-G).

**CRT deficiency induced numerous transcriptional changes to genes within the calcium signaling pathway**

As noted in Figures 4 and 6, some of the measured differences between CRT-KO and parental cells are not fully reversed by reconstitution with wild-type CRT, although the trends are maintained. We predicted that there may be other indirect effects of CRT-KO and reconstitution that affect cellular calcium levels and calcium signaling that could explain some of these measured differences. As proof of concept, we undertook bulk RNA-sequencing to determine differential gene expression in MEG-01 parental *vs.* CRT-KO cells. There were 3078 upregulated and 1790 downregulated genes. The volcano plot and heat map show identified genes that were differentially expressed in CRT-KO MEG-01 compared to parental cells (Figure 7A). Based on pathway analysis, numerous genes involved in cellular calcium signaling were identified. Of specific note is the upregulation of GRP94 encoded by the *HSP90B1* gene, BiP encoded by *HSPA5* gene, and PDIA6 encoded by *PDIA6* gene, which are known to have low affinity calcium binding sites (Lievremont et al., 1997, Macer and Koch, 1988, Biswas et al., 2007, Marzec et al., 2012, Okumura et al., 2021) (Figures 7A and 7B). Other studies have reported similar upregulation of these genes in CRT-KO (Tang et al., 2025) as well as in heterozygous $CRT_{Del52}$ knock-in cells (Figure 7C) (Fosselteder et al., 2023). Upregulation of these proteins may serve a compensatory role in buffering calcium in CRT-KO cells. Additionally, PDIA3, which is shown to regulate the activities of stromal interaction molecule 1 (STIM1) (Prins et al., 2011) and Sarco/endoplasmic reticulum $Ca^{2+}$ ATPase (SERCA2b) (Li and Camacho, 2004), was consistently upregulated in all the studies.

We further used real-time PCR with target gene primers (Supplementary Table 2) to validate the expression of the key ER resident proteins identified from the RNA-sequencing data which have roles in calcium binding and regulation of ER calcium homeostasis. Consistent with the RNA-seq data, the expression of *HSPA5, HSP90B1, PDIA6* and *PDIA3* mRNA transcripts was significantly increased in CRT-KO MEG-01 compared to parental cells. Reconstitution of CRT-KO cells with wild-type CRT but not $CRT_{Del52}$ showed a significant decrease in the expression of *HSPA5, HSP90B1, PDIA6 and PDIA3* (Figures 7D-G). Protein levels of BiP, GRP94, PDIA6 and PDIA3 were also assessed in the indicated cells by immunoblots using specific antibodies (supplementary methods). Representative immunoblots show increased expression of BiP (Figure 7D, right panel), GRP94 (Figure 7E, right panel), PDIA6 (Figure 7F, right panel) and PDIA3 (Figure 7G, right panel) in CRT-KO cells compared to parental MEG-01 cells as well as increased expression in CRT-KO-Vec cells compared to CRT-KO cells reconstituted with wild type CRT. The effects of $CRT_{Del52}$ in reducing expression were generally less robust than wild type CRT.

## Discussion

Calreticulin is a ubiquitously expressed ER luminal calcium-binding chaperone, with a role in ER calcium storage (Venkatesan et al., 2021b, Michalak, 2024). Previous studies using dye-based assays reported impaired calcium binding by the MPN-associated $CRT_{Del52}$ mutant (Ibarra et al., 2022). Yet direct and quantitative analyses of its calcium-binding properties have been lacking. In this study, we investigated low affinity calcium binding by wild-type human CRT, $CRT_{Del52}$, and the truncation mutants $CRT_{(1-351)}$ and $CRT_{(1-339)}$ using ITC (Figure 3 and Table 1). Our studies show that wild-type CRT, $CRT_{Del52,}$ and $CRT_{(1-351)}$ retain low affinity calcium binding sites, exhibiting average $K_D$ values of 574.24, 938.82, and 444.34 μM, respectively. On the other hand, low affinity calcium binding by $CRT_{(1-339)}$ could not be reliably fit. This is the first quantitative characterization of the low affinity calcium binding profiles of wild-type human CRT, $CRT_{Del52}$, and functionally informative truncation mutants.

Although $CRT_{Del52}$ retains at least partial low affinity calcium binding capability, loss of its KDEL retention sequence (Figure 1) could still disrupt ER calcium storage and signaling. Interestingly, the cellular assays reveal that ER and cytosolic calcium levels, as well as SOCE, are similar between CRT-KO cells and those reconstituted with either wild-type CRT or $CRT_{Del52}$ (Figures 4-6). One study has reported decreased ER calcium levels in a human osteosarcoma cell line expressing $CRT_{Del52}$ compared to those expressing wild-type CRT, following transient transfections (Ibarra et al., 2022). The same study suggested the contributions of the P and C-domain of wild-type in restoring ER calcium levels in cells expressing $CRT_{Del52}$ (Ibarra et al., 2022). While the conditions of those experiments differ from the studies described here which use a CRT-KO background, our findings are consistent with the prediction that any excess free ER calcium generated in cells lacking CRT or sufficient ER calcium binding sites would rapidly diffuse out of the ER and be pumped out of the cell.

Related to cytosolic calcium levels and SOCE activation, consistent with our findings (Figure 6G), a previous study found no differences in cytosolic calcium levels or SOCE induction in myeloid progenitor 32D cells expressing wild-type CRT and $CRT_{Del52}$ both under conditions of cytokine deprivation and thrombopoietin (TPO) stimulation (Bhuria et al., 2024). While cultured megakaryocytes from MPN patients with *CALR* mutations have SOCE abnormalities compared to healthy control cells (Pietra et al., 2016, Di Buduo et al., 2020) sample to sample heterogeneities in primary cells make it difficult to attribute measured differences solely to calcium binding by CRT or its mutants.

We found that CRT-KO HEK cells displayed lower ER calcium compared with the parental HEK cells (Figure 4D, left panel) and also that CRT-KO Meg-01 cells displayed increased cytosolic calcium in the absence of extracellular calcium (Figure 6B). However, reconstitutions with wild-type CRT did not reverse these effects (Figure 4D, right panel and Figure 6E). Transcriptomic analysis identified significant alterations in the expression of genes related to calcium storage and signaling between parental and CRT-KO Meg-01 cells (Figure 7). These changes highlight adaptive or compensatory pathways induced by CRT-KO and emphasize that, when comparing wild-type and CRT-KO cell lines for subcellular calcium levels or responses to SERCA inhibitors, the measured effects might not be based solely on the abilities of CRT to maintain ER and cytosolic $Ca^{2+}$ levels via its calcium binding, storage and buffering capacity. Rather, many other compensatory cellular changes could affect subcellular calcium levels and signaling. In this study, various ER proteins with known calcium binding activities were found to be upregulated in CRT-KO cells (Figure 7A and 7B). GRP94 (Macer and Koch, 1988, Biswas et al., 2007, Marzec et al., 2012), BiP ((Lievremont et al., 1997) and our unpublished findings), and PDIA6 (Okumura et al., 2021) are each known to contain low affinity calcium binding sites. CRT-KO cells have significantly induced expression of the genes encoding these proteins. Wild type CRT

reconstitution into the CRT-KO cells significantly reduced the expression of these ER proteins, whereas $CRT_{Del52}$ reconstitution only partly and non-significantly reduced expression of *HSP90B1* and *PDIA6* and did not reduce the expression of *HSPA5* (Figures 7D-F). GRP94, BiP and PDIA6 have functions in ER protein folding and quality control (Hendershot et al., 2024, Okumura et al., 2021). It is known that $CRT_{Del52}$ has impaired chaperone activity towards its substrates compared with wild type CRT (Arshad and Cresswell, 2018, Schurch et al., 2022, Kaur et al., 2025). This could account for some of these measured differences between wild type CRT and $CRT_{Del52}$ in altering the expression of the ER chaperones and folding factors. However, their induction in knock-in cells with heterozygous expression of wild type CRT and $CRT_{Del52}$ (Fosselteder et al., 2023), in which the expressed wild type CRT appears sufficient for multiple protein folding activities (Kaur et al., 2025, Schurch et al., 2022) could point to compensatory effects relevant to calcium signaling. Regardless of the precise mechanisms relevant to induction of the calcium binding proteins, their combined expression, despite protein compositional differences between the KO and reconstituted cells, appears sufficient to maintain ER calcium levels (Figure 4D, right panel), calcium release from the ER (Figure 4E, right panel, and 5F) and cytosolic calcium levels (Figure 5E).

PDIA3 (ERp57) forms a complex with CRT and interacts with and regulates the activities of the ubiquitously expressed SERCA2b (Li and Camacho, 2004). Its expression is also induced by the CRT-KO and suppressed by wild type CRT expression but non-significantly by $CRT_{Del52}$ expression. Altered SERCA2b activity could also affect basal ER calcium levels, contributing to similarities between CRT-KO, and wild type CRT or $CRT_{Del52}$ reconstituted cells.

Collectively, our findings reveal that $CRT_{Del52}$ retains some ability to bind calcium at low affinity sites. CRT-KO cells reconstituted with wild-type or $CRT_{Del52}$ have comparable ER and cytosolic calcium levels and store-operated calcium entry (SOCE). CRT-KO induces broad changes in ER calcium binding protein expression as well as in the expression of ERp57. Overall, we can conclude that a number of factors that contribute to the maintenance of ER calcium levels and regulation of calcium transport into the ER are altered in CRT-KO cells. Thus, any disease-related changes in calcium signaling and homeostasis are likely multifactorial, encompassing transcriptional regulation and altered expression of critical mediators of calcium storage, transport and signaling pathways. These studies provide a more nuanced understanding of CRT's role in cellular calcium signaling and may inform future therapeutic strategies targeting calcium signaling pathways in hematological malignancies.

409

**Acknowledgements**

We thank Grace Pagnucco for her contribution to creating the CRISPR/Cas9-engineered HEK293T CRT-KO cells and Arunkumar Venkatesan for the MEG-01 CRT-KO cells. We would like to extend special thanks and appreciation to Chante Liu and Mathewos Biniam Tebeje from the Satin lab for their support with microscopic calcium measurements. We thank Luis Teran-Rodriguez for assistance with data analysis and Dr. Sivaraj Sivaramakrishnan for many helpful suggestions.

We thank the Advanced Genomic Core (ACG) at the University of Michigan for conducting the library preparation and next-generation sequencing, as well as Rebecca Tagett and the Bioinformatics Core of the University of Michigan Medical School for conducting the RNA sequencing data analysis. We thank Dr. Arthur Sherman for many insightful comments. This work was funded by the National Institute of Health grants (R01 AI123957 to MR and R01DK46409 to LSS) and by the University of Michigan Fast Forward Protein Folding Diseases Initiative.

# REFERENCES

## Uncategorized References


ARAKI, M., YANG, Y., MASUBUCHI, N., HIRONAKA, Y., TAKEI, H., MORISHITA, S., MIZUKAMI, Y., KAN, S., SHIRANE, S., EDAHIRO, Y., SUNAMI, Y., OHSAKA, A. & KOMATSU, N. 2016. Activation of the thrombopoietin receptor by mutant calreticulin in CALR-mutant myeloproliferative neoplasms. *Blood,* 127**,** 1307-16.

ARSHAD, N. & CRESSWELL, P. 2018. Tumor-associated calreticulin variants functionally compromise the peptide loading complex and impair its recruitment of MHC-I. *J Biol Chem,* 293**,** 9555-9569.

BAGUR, R. & HAJNOCZKY, G. 2017. Intracellular Ca(2+) Sensing: Its Role in Calcium Homeostasis and Signaling. *Mol Cell,* 66**,** 780-788.

BAKSH, S. & MICHALAK, M. 1991. Expression of Calreticulin in Escherichia-Coli and Identification of Its Ca2+ Binding Domains. *Journal of Biological Chemistry,* 266**,** 21458-21465.

BHURIA, V., FRANZ, T., BALDAUF, C., BOTTCHER, M., CHATAIN, N., KOSCHMIEDER, S., BRUMMENDORF, T. H., MOUGIAKAKOS, D., SCHRAVEN, B., KAHLFUSS, S. & FISCHER, T. 2024. Activating mutations in JAK2 and CALR differentially affect intracellular calcium flux in store operated calcium entry. *Cell Commun Signal,* 22**,** 186.

BISWAS, C., OSTROVSKY, O., MAKAREWICH, C. A., WANDERLING, S., GIDALEVITZ, T. & ARGON, Y. 2007. The peptide-binding activity of GRP94 is regulated by calcium. *Biochem J,* 405**,** 233-41.

CHACHOUA, I., PECQUET, C., EL-KHOURY, M., NIVARTHI, H., ALBU, R. I., MARTY, C., GRYSHKOVA, V., DEFOUR, J. P., VERTENOEIL, G., NGO, A., KOAY, A., RASLOVA, H., COURTOY, P. J., CHOONG, M. L., PLO, I., VAINCHENKER, W., KRALOVICS, R. & CONSTANTINESCU, S. N. 2016. Thrombopoietin receptor activation by myeloproliferative neoplasm associated calreticulin mutants. *Blood,* 127**,** 1325-35.

DEL CID, N., JEFFERY, E., RIZVI, S. M., STAMPER, E., PETERS, L. R., BROWN, W. C., PROVODA, C. & RAGHAVAN, M. 2010. Modes of calreticulin recruitment to the major histocompatibility complex class I assembly pathway. *J Biol Chem,* 285**,** 4520-35.

DELPROPOSTO, J., MAJMUDAR, C. Y., SMITH, J. L. & BROWN, W. C. 2009. Mocr: a novel fusion tag for enhancing solubility that is compatible with structural biology applications. *Protein Expr Purif,* 63**,** 40-9.

DI BUDUO, C. A., ABBONANTE, V., MARTY, C., MOCCIA, F., RUMI, E., PIETRA, D., SOPRANO, P. M., LIM, D., CATTANEO, D., IURLO, A., GIANELLI, U., BAROSI, G., ROSTI, V., PLO, I., CAZZOLA, M. & BALDUINI, A. 2020. Defective interaction of mutant calreticulin and SOCE in megakaryocytes from patients with myeloproliferative neoplasms. *Blood,* 135**,** 133-144.

FOSSELTEDER, J., PABST, G., SCONOCCHIA, T., SCHLACHER, A., AUINGER, L., KASHOFER, K., BEHAM-SCHMID, C., TRAJANOSKI, S., WASKOW, C., SCHOLL, W., SILL, H., ZEBISCH, A., WOLFLER, A., THOMAS, D. & REINISCH, A. 2023. Human gene-engineered calreticulin mutant stem cells recapitulate MPN hallmarks and identify targetable vulnerabilities. *Leukemia,* 37**,** 843-853.

HAN, L., SCHUBERT, C., KOHLER, J., SCHEMIONEK, M., ISFORT, S., BRUMMENDORF, T. H., KOSCHMIEDER, S. & CHATAIN, N. 2016. Calreticulin-mutant proteins induce megakaryocytic signaling to transform hematopoietic cells and undergo accelerated degradation and Golgi-mediated secretion. *J Hematol Oncol,* 9**,** 45.

HENDERSHOT, L. M., BUCK, T. M. & BRODSKY, J. L. 2024. The Essential Functions of Molecular Chaperones and Folding Enzymes in Maintaining Endoplasmic Reticulum Homeostasis. *J Mol Biol,* 436**,** 168418.

IBARRA, J., ELBANNA, Y. A., KURYLOWICZ, K., CIBODDO, M., GREENBAUM, H. S., ARELLANO, N. S., RODRIGUEZ, D., EVERS, M., BOCK-HUGHES, A., LIU, C., SMITH, Q., LUTZE, J., BAUMEISTER, J., KALMER, M., OLSCHOK, K., NICHOLSON, B., SILVA, D., MAXWELL, L., DOWGIELEWICZ, J., RUMI, E., PIETRA, D., CASETTI, I. C., CATRICALA, S., KOSCHMIEDER, S., GURBUXANI, S., SCHNEIDER, R. K., OAKES, S. A. & ELF, S. E. 2022. Type I but Not Type II Calreticulin Mutations Activate the IRE1alpha/XBP1 Pathway of the Unfolded Protein Response to Drive Myeloproliferative Neoplasms. *Blood Cancer Discov,* 3**,** 298-315.

KAUR, A., DESIKAN, H., PAGNUCCO, G., KANDARPA, M., TALPAZ, M. & RAGHAVAN, M. 2025. Effects of Calreticulin Mutations on HLA Class I Expression in Myeloproliferative Neoplasms. *bioRxiv*.

KLAMPFL, T., GISSLINGER, H., HARUTYUNYAN, A. S., NIVARTHI, H., RUMI, E., MILOSEVIC, J. D., THEM, N. C., BERG, T., GISSLINGER, B., PIETRA, D., CHEN, D., VLADIMER, G. I., BAGIENSKI, K., MILANESI, C., CASETTI, I. C., SANT'ANTONIO, E., FERRETTI, V., ELENA, C., SCHISCHLIK, F., CLEARY, C., SIX, M., SCHALLING, M., SCHONEGGER, A., BOCK, C., MALCOVATI, L., PASCUTTO, C., SUPERTI-FURGA, G., CAZZOLA, M. & KRALOVICS, R. 2013. Somatic mutations of calreticulin in myeloproliferative neoplasms. *N Engl J Med,* 369**,** 2379-90.

LI, J., PRINS, D., PARK, H. J., GRINFELD, J., GONZALEZ-ARIAS, C., LOUGHRAN, S., DOVEY, O. M., KLAMPFL, T., BENNETT, C., HAMILTON, T. L., PASK, D. C., SNEADE, R., WILLIAMS, M., AUNGIER, J., GHEVAERT, C., VASSILIOU, G. S., KENT, D. G. & GREEN, A. R. 2018. Mutant calreticulin knockin mice develop thrombocytosis and myelofibrosis without a stem cell self-renewal advantage. *Blood,* 131**,** 649-661.

LI, Y. & CAMACHO, P. 2004. Ca2+-dependent redox modulation of SERCA 2b by ERp57. *J Cell Biol,* 164**,** 35-46.

LIEVREMONT, J. P., RIZZUTO, R., HENDERSHOT, L. & MELDOLESI, J. 1997. BiP, a major chaperone protein of the endoplasmic reticulum lumen, plays a direct and important role in the storage of the rapidly exchanging pool of Ca2+. *J Biol Chem,* 272**,** 30873-9.

LIU, P., ZHAO, L., LOOS, F., MARTY, C., XIE, W., MARTINS, I., LACHKAR, S., QU, B., WAECKEL-ENEE, E., PLO, I., VAINCHENKER, W., PEREZ, F., RODRIGUEZ, D., LOPEZ-OTIN, C., VAN ENDERT, P., ZITVOGEL, L., KEPP, O. & KROEMER, G. 2020. Immunosuppression by Mutated Calreticulin Released from Malignant Cells. *Mol Cell,* 77**,** 748-760 e9.

MACER, D. R. & KOCH, G. L. 1988. Identification of a set of calcium-binding proteins in reticuloplasm, the luminal content of the endoplasmic reticulum. *J Cell Sci,* 91 ( Pt 1)**,** 61-70.

MARTY, C., PECQUET, C., NIVARTHI, H., EL-KHOURY, M., CHACHOUA, I., TULLIEZ, M., VILLEVAL, J. L., RASLOVA, H., KRALOVICS, R., CONSTANTINESCU, S. N., PLO, I. & VAINCHENKER, W. 2016. Calreticulin mutants in mice induce an MPL-dependent thrombocytosis with frequent progression to myelofibrosis. *Blood,* 127**,** 1317-24.

MARZEC, M., ELETTO, D. & ARGON, Y. 2012. GRP94: An HSP90-like protein specialized for protein folding and quality control in the endoplasmic reticulum. *Biochim Biophys Acta,* 1823**,** 774-87.

MASUBUCHI, N., ARAKI, M., YANG, Y., HAYASHI, E., IMAI, M., EDAHIRO, Y., HIRONAKA, Y., MIZUKAMI, Y., KIHARA, Y., TAKEI, H., NUDEJIMA, M., KOIKE, M., OHSAKA, A. & KOMATSU, N. 2020. Mutant calreticulin interacts with MPL in the secretion pathway for activation on the cell surface. *Leukemia,* 34**,** 499-509.

MICHALAK, M. 2024. Calreticulin: Endoplasmic reticulum Ca(2+) gatekeeper. *J Cell Mol Med,* 28**,** e17839.

NAKAMURA, K., ZUPPINI, A., ARNAUDEAU, S., LYNCH, J., AHSAN, I., KRAUSE, R., PAPP, S., DE SMEDT, H., PARYS, J. B., MULLER-ESTERL, W., LEW, D. P., KRAUSE, K. H., DEMAUREX, N., OPAS, M. & MICHALAK, M. 2001. Functional specialization of calreticulin domains. *J Cell Biol,* 154**,** 961-72.

NANGALIA, J., MASSIE, C. E., BAXTER, E. J., NICE, F. L., GUNDEM, G., WEDGE, D. C., AVEZOV, E., LI, J., KOLLMANN, K., KENT, D. G., AZIZ, A., GODFREY, A. L., HINTON, J., MARTINCORENA, I., VAN LOO, P., JONES, A. V., GUGLIELMELLI, P., TARPEY, P., HARDING, H. P., FITZPATRICK, J. D., GOUDIE, C. T., ORTMANN, C. A., LOUGHRAN, S. J., RAINE, K., JONES, D. R., BUTLER, A. P., TEAGUE, J. W., O'MEARA, S., MCLAREN, S., BIANCHI, M., SILBER, Y., DIMITROPOULOU, D., BLOXHAM, D., MUDIE, L., MADDISON, M., ROBINSON, B., KEOHANE, C., MACLEAN, C., HILL, K., ORCHARD, K., TAURO, S., DU, M. Q., GREAVES, M., BOWEN, D., HUNTLY, B. J. P., HARRISON, C. N., CROSS, N. C. P., RON, D., VANNUCCHI, A. M., PAPAEMMANUIL, E., CAMPBELL, P. J. & GREEN, A. R. 2013. Somatic CALR mutations in myeloproliferative neoplasms with nonmutated JAK2. *N Engl J Med,* 369**,** 2391-2405.

OKUMURA, M., KANEMURA, S., MATSUSAKI, M., KINOSHITA, M., SAIO, T., ITO, D., HIRAYAMA, C., KUMETA, H., WATABE, M., AMAGAI, Y., LEE, Y. H., AKIYAMA, S. & INABA, K. 2021. A unique leucine-valine adhesive motif supports structure and function of protein disulfide isomerase P5 via dimerization. *Structure,* 29**,** 1357-1370 e6.

PECQUET, C., PAPADOPOULOS, N., BALLIGAND, T., CHACHOUA, I., TISSERAND, A., VERTENOEIL, G., NEDELEC, A., VERTOMMEN, D., ROY, A., MARTY, C., NIVARTHI, H., DEFOUR, J. P., EL-KHOURY, M., HUG, E., MAJOROS, A., XU, E., ZAGRIJTSCHUK, O., FERTIG, T. E., MARTA, D. S., GISSLINGER, H., GISSLINGER, B., SCHALLING, M., CASETTI, I., RUMI, E., PIETRA, D., CAVALLONI, C., ARCAINI, L., CAZZOLA, M., KOMATSU, N., KIHARA, Y., SUNAMI, Y., EDAHIRO, Y., ARAKI, M., LESYK, R., BUXHOFER-AUSCH, V., HEIBL, S., PASQUIER, F., HAVELANGE, V., PLO, I., VAINCHENKER, W., KRALOVICS, R. & CONSTANTINESCU, S. N. 2023. Secreted mutant calreticulins as rogue cytokines in myeloproliferative neoplasms. *Blood,* 141**,** 917-929.

PIETRA, D., RUMI, E., FERRETTI, V. V., DI BUDUO, C. A., MILANESI, C., CAVALLONI, C., SANT'ANTONIO, E., ABBONANTE, V., MOCCIA, F., CASETTI, I. C., BELLINI, M., RENNA, M. C., RONCORONI, E., FUGAZZA, E., ASTORI, C., BOVERI, E., ROSTI, V., BAROSI, G., BALDUINI, A. & CAZZOLA, M. 2016. Differential clinical effects of different mutation subtypes in CALR-mutant myeloproliferative neoplasms. *Leukemia,* 30**,** 431-8.

PRINS, D., GROENENDYK, J., TOURET, N. & MICHALAK, M. 2011. Modulation of STIM1 and capacitative Ca2+ entry by the endoplasmic reticulum luminal oxidoreductase ERp57. *EMBO Rep,* 12**,** 1182-8.

PUTNEY, J. W. 2011. Origins of the concept of store-operated calcium entry. *Front Biosci (Schol Ed),* 3**,** 980-4.

SCHURCH, P. M., MALINOVSKA, L., HLEIHIL, M., LOSA, M., HOFSTETTER, M. C., WILDSCHUT, M. H. E., LYSENKO, V., LAKKARAJU, A. K. K., MAAT, C. A., BENKE, D., AGUZZI, A., WOLLSCHEID, B., PICOTTI, P. & THEOCHARIDES, A. P. A. 2022. Calreticulin mutations affect its chaperone function and perturb the glycoproteome. *Cell Rep,* 41**,** 111689.

SHIVAROV, V., IVANOVA, M. & TIU, R. V. 2014. Mutated calreticulin retains structurally disordered C terminus that cannot bind Ca(2+): some mechanistic and therapeutic implications. *Blood Cancer J,* 4**,** e185.

SUZUKI, J., KANEMARU, K., ISHII, K., OHKURA, M., OKUBO, Y. & IINO, M. 2014. Imaging intraorganellar Ca2+ at subcellular resolution using CEPIA. *Nat Commun,* 5**,** 4153.

TANG, K., WU, L., HU, Y., XUE, T., JIN, Y., ZHOU, X., LUO, C., ZHAO, Y., TONG, L., DAI, J., FENG, D., ZENG, Z. & PAN, D. 2025. Perturbation of calreticulin potentiates CD8+ T cell-mediated antitumor immunity. *J Exp Med,* 222.

VENKATESAN, A., GENG, J., KANDARPA, M., WIJEYESAKERE, S. J., BHIDE, A., TALPAZ, M., POGOZHEVA, I. D. & RAGHAVAN, M. 2021a. Mechanism of mutant calreticulin-mediated activation of the thrombopoietin receptor in cancers. *J Cell Biol,* 220.

VENKATESAN, A., SATIN, L. S. & RAGHAVAN, M. 2021b. Roles of Calreticulin in Protein Folding, Immunity, Calcium Signaling and Cell Transformation. *Prog Mol Subcell Biol,* 59**,** 145-162.

WIJEYESAKERE, S. J., BEDI, S. K., HUYNH, D. & RAGHAVAN, M. 2016. The C-Terminal Acidic Region of Calreticulin Mediates Phosphatidylserine Binding and Apoptotic Cell Phagocytosis. *J Immunol,* 196**,** 3896-3909.

WIJEYESAKERE, S. J., GAFNI, A. A. & RAGHAVAN, M. 2011. Calreticulin is a thermostable protein with distinct structural responses to different divalent cation environments. *J Biol Chem,* 286**,** 8771-85.

ZHANG, I. X., RAGHAVAN, M. & SATIN, L. S. 2020. The Endoplasmic Reticulum and Calcium Homeostasis in Pancreatic Beta Cells. *Endocrinology,* 161.

## Figures and legends

```
mCRT      DGEWEPPVIQNPEYKGEWKPRQIDNPDYKGTWIHPEIDNPEYSPDANIYAYDSFAVLGLD 300
hCRT      DGEWEPPVIQNPEYKGEWKPRQIDNPDYKGTWIHPEIDNPEYSPDPSIYAYDNFGVLGLD 300
Ins5      DGEWEPPVIQNPEYKGEWKPRQIDNPDYKGTWIHPEIDNPEYSPDPSIYAYDNFGVLGLD 300
Del52     DGEWEPPVIQNPEYKGEWKPRQIDNPDYKGTWIHPEIDNPEYSPDPSIYAYDNFGVLGLD 300
          ********************************************* .*****.*.*****

                                                  340       349
mCRT      LWQVKSGTIFDNFLITNDEAYAEEFGNETWGVTKAAEKQMKDKQDEEQRLKEEEEDKKRK 360
hCRT      LWQVKSGTIFDNFLITNDEAYAEEFGNETWGVTKAAEKQMKDKQDEEQRLKEEEEDKKRK 360
Ins5      LWQVKSGTIFDNFLITNDEAYAEEFGNETWGVTKAAEKQMKDKQDEEQRLKEEEEDKKRK 360
Del52     LWQVKSGTIFDNFLITNDEAYAEEFGNETWGVTKAAEKQMKDKQDEEQR----------- 349
          ************************************************

mCRT      EEEEAEDKEDDDDRDEDEDEEDEK---EEDEEESPGQAKDEL-----------  399
hCRT      EEEEAEDKEDDEDKDEDEEDEEDK--EEDEEEDVPGQAKDEL-----------  400
Ins5      EEEEAEDNCRRMMRTKMRMRRMRRTRRKMRRKMSPARPRTSCREACLQGWTEA  413
Del52     --------TRRMMRTKMRMRRMRRTRRKMRRKMSPARPRTSCREACLQGWTEA  394
```

**Figure 1: Sequence alignments of the C-terminal residues of murine and human calreticulin (mCRT and hCRT), MPN-linked CRT mutants Ins5 and Del52.** Multiple sequence alignment using Clustal Omega was employed to compare C-domain sequences of mature mCRT, hCRT, Del52, and Ins5 proteins. Acidic residues (340 – 349) previously implicated in low affinity calcium binding by mCRT that are shared between wild-type and both $CRT_{Del52}$ and $CRT_{Ins5}$ are highlighted in green. Additional acidic residues shared just between wild-type CRT and $CRT_{Ins5}$ are shown in red. There are additional acidic residues unique to wild-type CRT. Mature protein numbering is used for the CRT sequences.

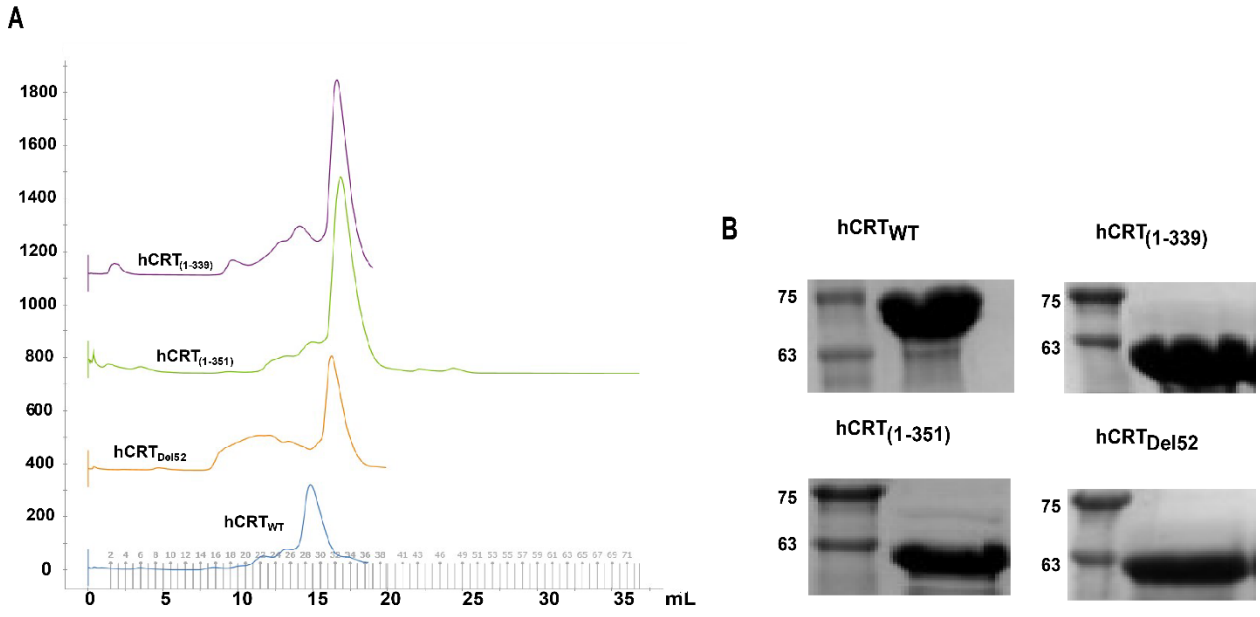


**Figure 2**: **Purification of recombinant human wild-type CRT, $CRT_{Del52}$, and C-domain truncation mutants. A)** Representative chromatograms of recombinant GB1-and his-tagged human $CRT_{WT}$ ($hCRT_{WT}$), $CRT_{Del52}$, and the C-domain truncation mutants hCRT $_{(1-351)}$ and hCRT $_{(1-339)}$ purified by gel exclusion chromatography after expression in *E. coli* and initial purification using a nickel resin. **B)** Representative Coomassie blue-stained SDS-PAGE gels of purified proteins that were used for calcium-binding measurements.

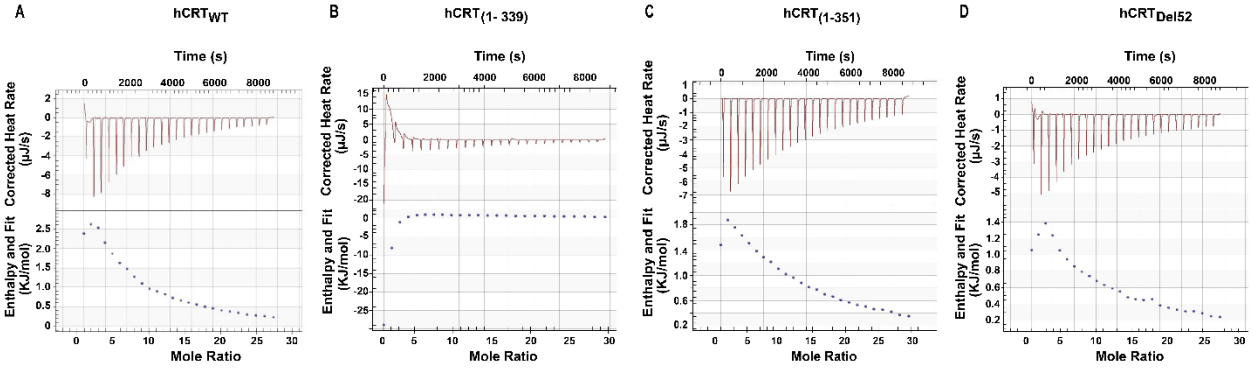


**Figure 3: Calcium binding to the low affinity sites of purified human CRT proteins.** Low affinity calcium binding by purified $hCRT_{WT}$, $CRT_{Del52}$, and the indicated truncation mutants was measured using isothermal titration calorimetry. **A-D)** Representative isotherm and fitting curves of calcium binding to the low affinity sites of the wild-type and mutant CRT proteins as indicated, measured using isothermal titration calorimetry (ITC). Prior to titration, the proteins were incubated with 50-100 µM $CaCl_2$ to block the high affinity calcium binding sites. At 37°C, 10 mM $CaCl_2$ was titrated against 100 µM protein. The heat change was measured for 25 injections, and the data were curve-fitted to calculate the dissociation constant, enthalpy, and binding stoichiometry using NanoAnalyzer software. Data replicates and statistical analyses are specified in Table 1.

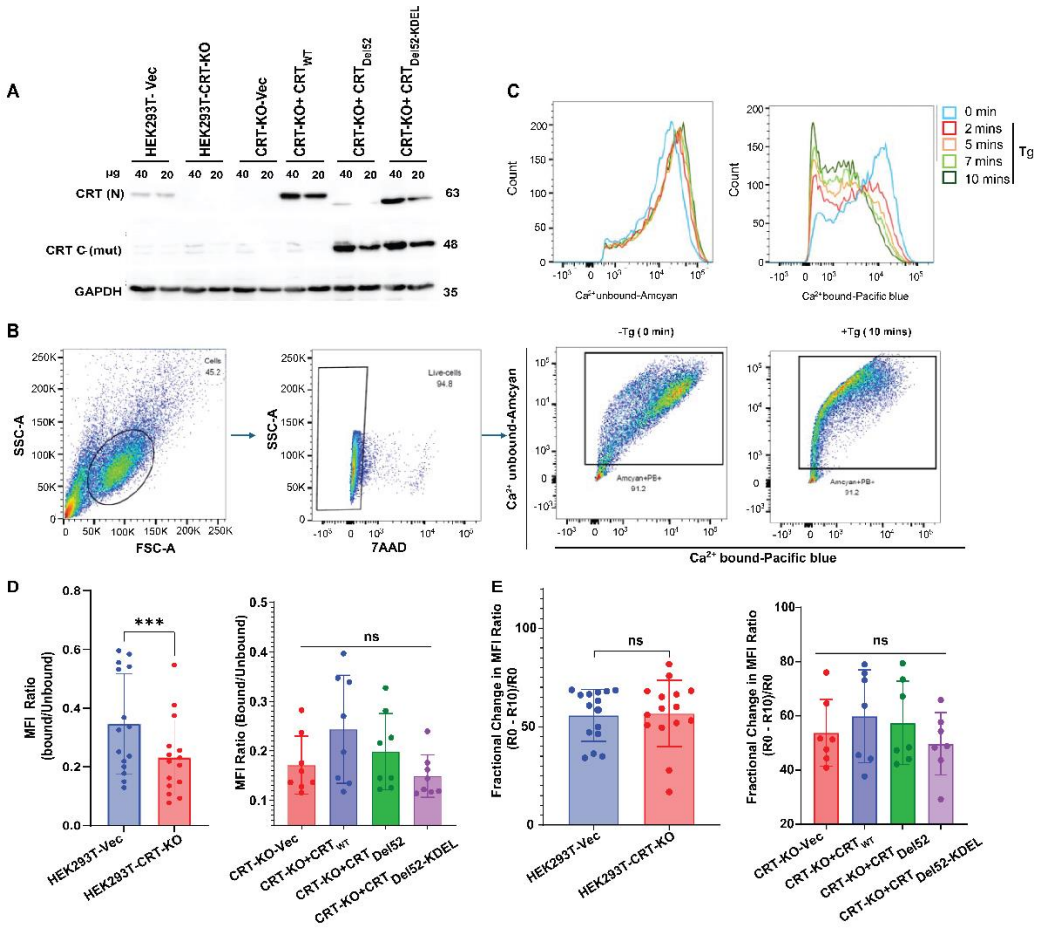


**Figure 4: ER calcium measurements in CRT-KO HEK293T cells and those reconstituted with wild-type CRT, $CRT_{Del52}$, or $CRT_{Del52\text{-}KDEL}$. A)** CRISPR-Cas9 editing of HEK cells using lentiviral constructs of calreticulin-targeting gRNA (CRT-KO) or empty vector (HEK-Vec). CRT-KO HEK cells were subsequently reconstituted with wild-type human CRT, $CRT_{Del52}$, or $CRT_{Del52}$ with a C-terminal KDEL sequence as indicated. Representative blots showing expression levels of CRT in the indicated HEK cells. Cell lysates were subjected to SDS-PAGE followed by immunoblotting. Wild-type CRT, mutant CRT, and GAPDH were detected with anti-CRT (N), anti-CRT C-(mut), and anti-GAPDH antibodies, respectively. **B)** Gating strategy for flow cytometry. HEK-Vec cells transiently transfected with the vector encoding the ratiometric GEM-CEPIA1er probe for 72 hours were used to assess ER calcium levels by flow cytometry based on the measurements of fluorescence emission signals for the $Ca^{2+}$- bound or unbound probe at 452-455 nm and 498 nm, respectively following excitation with the 405 nm (violet) laser. Transfected cells were gated based on forward (FSC-A) and side scatter (SSC-A), then on 7AAD-negative (live) cells, and further on the cells positive for the calcium-bound or unbound probe signals. Representative dot plots of changes in fluorescence intensities in response to treatment with thapsigargin (Tg), a SERCA inhibitor, before (0 mins) or after (10 mins) treatment, are shown. **C)** Representative histograms showing changes to $Ca^{2+}$-bound and unbound signals at different time points following Tg treatment of cells. Mean fluorescence intensities (MFI) for $Ca^{2+}$-bound and unbound signals were used to calculate the bound/unbound ratios at different time points. **D and E)** The basal free ER calcium signals were measured as bound/unbound MFIs ratios from the corresponding histograms of CRT-KO or HEK-Vec cells (D, left panel) or CRT-KO cells reconstituted with the indicated CRT constructs (D, right panel). The fractional changes in ER calcium signals in response to Tg were measured at different time points in the indicated cells (E). The fractional change ratios were normalized to the baseline and calculated by subtracting the ratio at 10 min from the ratio at 0 mins (R0-R10/R0)x100. Statistical significance was determined using GraphPad Prism and based on paired t-tests (left panels of D and E) or one-way ANOVA analyses with Tukey's test (right panels of D and E). ns, not significant; *** P value < 0.001. All measurements were undertaken in the presence of 2 mM extracellular $Ca^{2+}$. Data shown in D and E are based on 7-15 independent experiments as indicated by the individual data points within the graphs. GAPDH, glyceraldehyde-3-phosphate dehydrogenase; SDS-PAGE, sodium dodecyl sulfate-polyacrylamide gel electrophoresis.

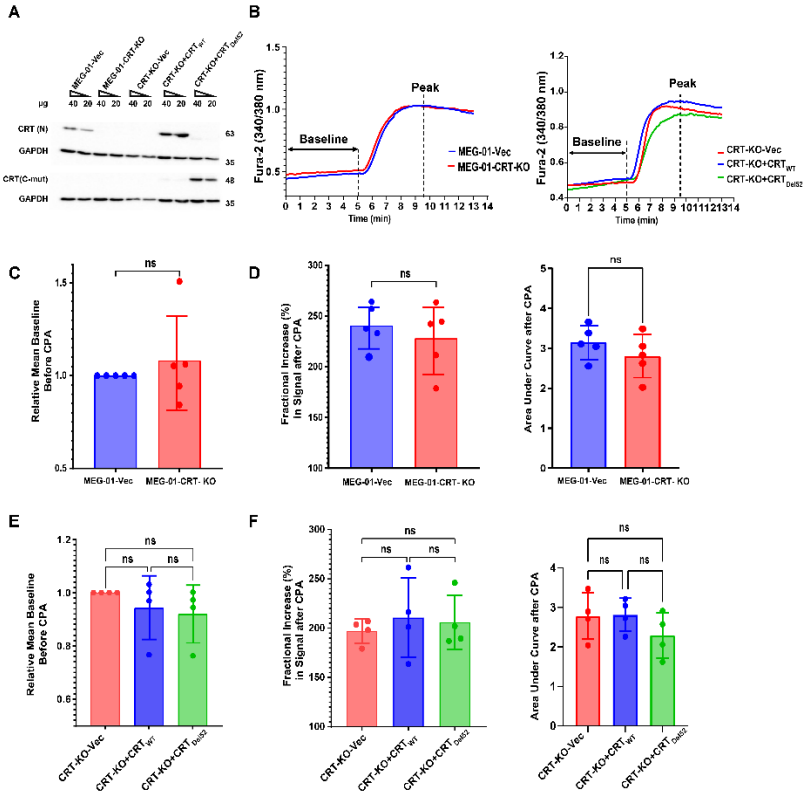


**Figure 5: Measurements of cytosolic calcium levels in megakaryoblastic (MEG-01) parental cells, CRT-KO cells, or those reconstituted with wild-type CRT or $CRT_{Del52}$** Cells in 2 mM extracellular $Ca^{2+}$ were loaded with the Fura-2/AM dye, and the ratio of the signals was calculated following excitation at 340 and 380 nm and emission at 510 nm. **A)** CRISPR-Cas9 editing of MEG-01 cells using lentiviral constructs encoding calreticulin-targeting gRNA (CRT-KO) or empty vector (Vec). CRT-KO MEG-01 cells were subsequently reconstituted with viral constructs encoding wild-type human CRT or $CRT_{Del52}$ or transduced with empty vector (Vec) as indicated in the Figure panels. Representative immunoblots of CRT expression in the indicated cells detected by the anti-CRT(N) and anti-CRT(C-mut) antibodies. **B)** Representative calcium imaging data from indicated cells in the presence of 2 mM extracellular $Ca^{2+}$ and following ER calcium depletion with SERCA inhibitor, cyclopiazonic acid (CPA). **C and E)** Basal cytosolic calcium levels were plotted as the means of ratios of emission signals following excitation at 340 and 380 nm. **D and F)** Fractional changes to cytosolic calcium levels in the indicated cell lines, measured following treatment with CPA and total calcium release determined as the area under the curve (AUC), are plotted relative to the baseline following CPA addition. Data shown in C-F are based on 4 or 5 independent measurements, each including 50-100 cells. A paired t-test was used to analyze the mean difference between two groups (C and D). Multiple comparisons among groups were analyzed using one-way ANOVA analyses with Tukey's test (E and F). Statistical significance was determined based p-value ≤ 0.05 using GraphPad Prism. ns, not significant.

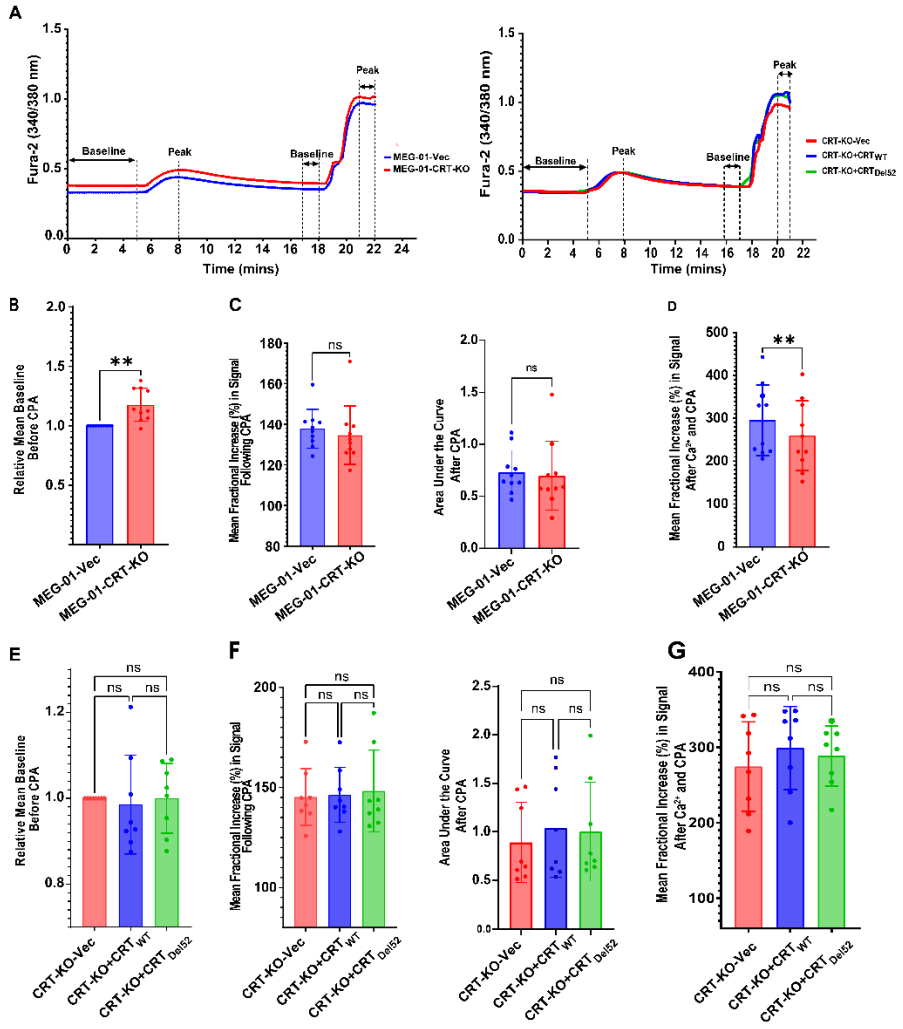


**Figure 6: Measurements of cytosolic calcium levels and SOCE in MEG-01 parental cells, CRT-KO, or those reconstituted with wild-type CRT or CRT$_{Del52}$.** Cells were loaded with Fura-2 dye, and the ratio of the 340 nm/380 nm signals was calculated following excitation at 340 and 380 nm and emission at 510 nm. **A)** Representative calcium imaging data from cells in the absence of extracellular calcium, followed by the addition of CPA, and subsequent addition of extracellular calcium with CPA as indicated. **B and E)** Compiled basal cytosolic calcium levels in the indicated cells in the absence of extracellular calcium plotted as the ratios of 340 nm/380 nm signals. **C and F)** Fractional changes to cytosolic calcium and total calcium release measured as the area under the curve (AUC) in the indicated cells following ER calcium depletion with the CPA. **D and G)** Fractional changes to cytosolic calcium following ER calcium depletion with the CPA and subsequent addition of extracellular calcium with CPA. Data are plotted as a fractional increase relative to baseline following CPA addition. SOCE in the indicated cells is plotted as the fractional increase in signal following the addition of 2 mM extracellular calcium in the presence of CPA. Data shown are based on 8-10 independent measurements, each with 20-100 cells. Comparisons were performed by paired t-test and one-way ANOVA analysis using GraphPad Prism. Statistical significance is based on a p-value ≤ 0.05. ns, not significant.

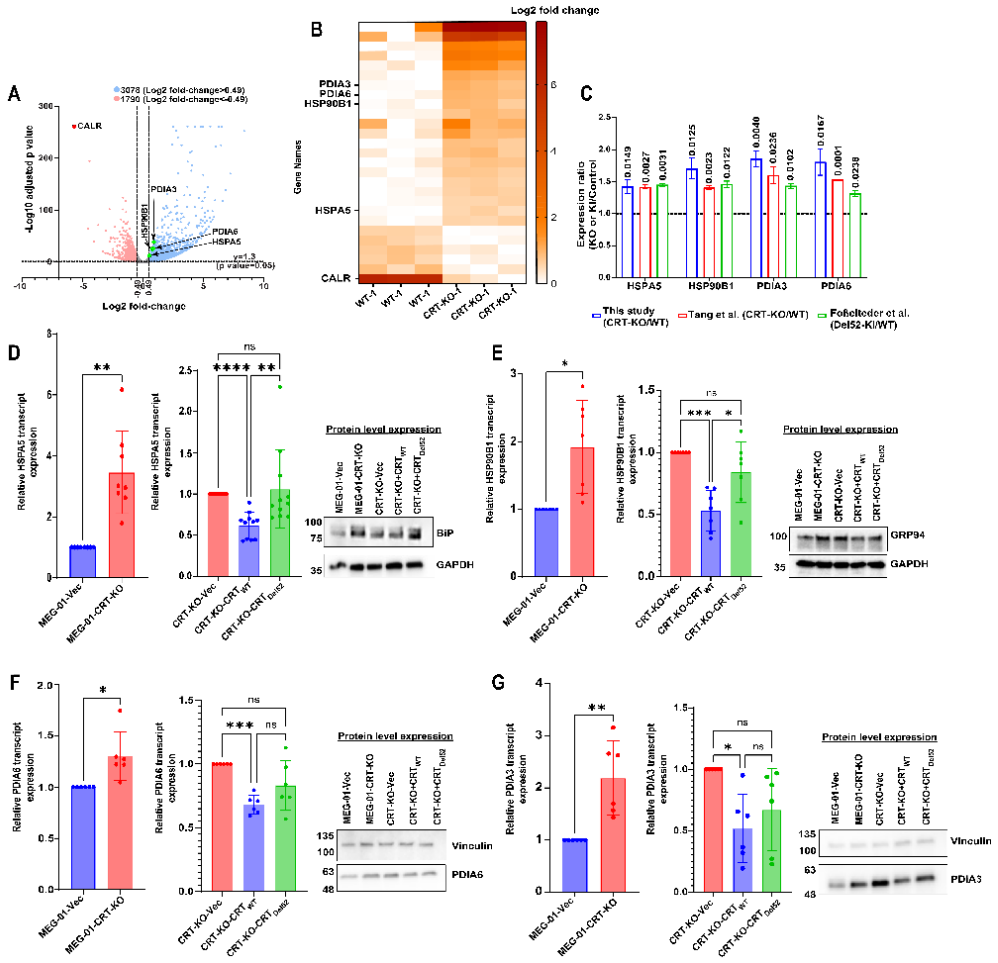


**Figure 7**: **Transcriptional changes to the expression of genes encoding ER calcium binding/regulating proteins in CRT-KO MEG-01 cells**. **A)** RNA sequencing analysis was used to identify differentially expressed genes in Meg-01 CRT-KO cells in comparison to parental Meg-01 cells. Volcano plot shows significantly upregulated (blue) and downregulated genes (red) genes identified by RNA sequencing. Genes related to ER calcium binding and homeostasis have been highlighted and labeled. The differentially expressed genes were selected as those with a log2 fold-change of <-0.49 or >0.49 and p values <0.05. **B)** Heat map shows the differential expression of genes encoding ER resident calcium binding proteins or ER calcium regulators that were identified by RNA sequencing in CRT-KO Meg-01 cells compared to parental cells (n=3 biological replicates). **C)** Comparison of expression ratio of *HSPA5, HSP90B1, PDIA3 and PDIA6* in CRT-KO Meg-01 cells (this study) or murine lung cancer cells (Tang et al., 2025) or heterozygous $CRT_{Del52}$ knock-in (Del52-KI) cells (Fosselteder et al., 2023) normalized to their expression in respective control cell lines expressing wild type CRT. The normalized expression of various genes identified in each dataset was calculated as a ratio of expression in CRT-KO or $CRT_{Del52}$ knock-in cells relative to the expression in wild-type CRT-expressing cells. Multiple unpaired t-tests were used to determine statistical significance with the Benjamini-Hochberg FDR correction (p-adjusted) <0.05. **D-G)** Left and middle panels: Relative expression of mRNA transcripts of *HSPA5* (n=8-11), *HSP90B1* (n=7), *PDIA6* (n=6) and *PDIA3* (n=6) genes in the indicated MEG-01 cells determined by RT-qPCR using specific gene primers. Relative gene expression was calculated by normalizing the target gene's cycle threshold (Ct) to a single or multiple endogenous controls (ACTB, GAPDH and HPRT1) which was used for comparison across different cell lines as indicated. Data show 6 - 11 independent runs with duplicate measurements for each run. Student t-test was used to determine the statistical significance between two groups while multiple group comparison was performed by one-way ANOVA analysis using GraphPad Prism. Statistical

significance is based on a p-value ≤ 0.05. ns, not significant. Right panels: Representative immunoblots of BiP, GRP94, PDIA6 and PDIA3 expression in the indicated cells detected by specific antibodies.

**Table 1:** Calorimetric data on measurement of calcium binding to the low affinity binding site of recombinant purified CRT.

| Recombinant CRT proteins/Isothermal calorimetric measurement | ΔH (k/mol) | n (mol) | Dissociation constant - $K_D$ (μM) |
|---|---|---|---|
| $CRT_{WT}$ | 7.88 ± 2.15 | 5.40 ± 1.31 | 574.24 ± 109.93 |
| $CRT_{(1-351)}$ | 79.82 ± 32.55 | 2.59 ± 1.56 | 444.34 ± 139.99 |
| $CRT_{(1-339)}$ | | | Too low to reliably fit |
| $CRT_{Del52}$ | 3.89 ± 1.36 | 7.73 ± 1.81 | 938.82 ± 275.89 |

Calorimetric data are represented as the mean ± S.E. Data shown are averages from 3 or 5 independent replicates.